*Article*

# Molecular Dynamics Simulation of Coiled Carbon Nanotube Pull-Out from Matrix

Feng Huang [1,2,3] and Shuai Zhou [1,*]

[1] College of Materials Science and Engineering, Chongqing University, Chongqing 400045, China
[2] State Key Laboratory of Mountain Bridge and Tunnel Engineering, Chongqing Jiaotong University, Chongqing 400074, China
[3] School of Civil Engineering, Chongqing Jiaotong University, Chongqing 400074, China
[*] Correspondence: shuaizhou@cqu.edu.cn

**Abstract:** The interaction between coiled carbon nanotubes (CCNT) and the polymer matrix is important in the mechanical, thermal, and electrical properties of the CCNT reinforced nanocomposite. In this study, molecular dynamics (MD) simulations were performed to study the interfacial characteristics of polymer nanocomposites (PNCs). Furthermore, the influence of the geometries of the CCNTs on the load transfer mechanism is evaluated. Pullout simulations considering different geometries of CCNTs are carried out to examine the tensile force and the interfacial shear stress (ISS). The results reveal that the maximal tensile force is reduced by increasing CCNT inner diameters, increasing the helix angles, and decreasing nanotube diameters. The distance between CCNTs and the polymer matrix is varied, and the interfacial distance favors greater ISS. Decreasing the inner diameter of the CCNT, the helix angle, and the tube diameter increases the ISS. The enhancement mechanism of CCNT/polymer composites has also been illustrated. Due to a lack of experimental results, only numerical results are given. The present study helps to understand the interfacial adhesion behavior between the polymer matrix and CCNTs and is expected to contribute to the development of CCNT reinforced polymer composites.

**Keywords:** composites; coiled carbon nanotubes; interfacial properties; molecular dynamics simulations

## 1. Introduction

Since their discovery in 1991, carbon nanotubes (CNTs) have attracted a lot of attention in most areas of science and engineering [1]. Compared with the straight CNTs, some other kinds of CNTs with curvature have received less attention. They have diverse morphologies as well as unique physical and chemical properties with the potential applications in engineering [2,3]. One kind of them is coiled carbon nanotubes (CCNTs). The straight and curved CNTs are planar structures, while CCNTs can spiral in three-dimensional space. CCNTs exhibit excellent mechanical and electrical properties because of the combination of coil morphology and properties of CNTs [4].

Some research has focused on the mechanical properties of CCNTs. A CCNT behaves like an elastic spring [5]. The CCNT-contained composite has great mechanical properties. Experimental results prove that CCNT/epoxy composites have great Vickers hardness values, Young's moduli, and tensile strengths. The performance of the CCNT/epoxy adhesive is outstanding due to the enhancement of the mechanical interlocking effect between CCNTs and epoxy. This effect leads to a greater Vickers hardness value, Young's modulus and lap joint shear strength when compared with the MWNT/epoxy type [6]. It is found that the elongation of the helical composite fibers can reach 100–300%, depending on the pitch of the helix and the tensile strain rate [7]. Meanwhile, molecular mechanics and molecular dynamics are used to investigate the elasticity, plasticity, vibration, and fracture of CCNTs [8–15]. The mechanical performance of CNT-reinforced composites is

significantly influenced by the interfacial properties between the CNT and the matrix [1]. A higher interfacial shear stress (ISS) leads to a better stress transfer from the polymer to the reinforcing CNTs [16]. Different parameters determine the reinforcement effect of the CNTs [17,18]. Several experimental studies have been conducted to investigate the interfacial characteristics of the CNT/polymer interface using both direct methods such as pullout or microdroplet tests, and indirect methods such as fragmentation tests or micro-Raman spectroscopy [19–23]. However, only a little research concentrates on the interfacial properties of the CCNT/polymer interface.

Determining their impact on the interfacial properties is essential in understanding how reinforcing mechanisms work. However, it is challenging to measure it experimentally via direct pullout tests [24]. As a result, different analytical and numerical techniques are considered to solve this problem. Some analytical models for the pullout process of wavy CNTs have been developed. The models are capable of predicting axial as well as interfacial shear stresses along a wavy CNT embedded in a matrix. Based on the pullout modeling technique, the effects of waviness, aspect ratio, CNT diameter, volume fraction, Poisson's ratio, and matrix modulus on axial and interfacial shear stresses have also been analyzed in detail [25,26]. With either a constant or Coulomb friction interface, the pull-out model predicts higher pullout forces as the fiber curvature increases, with zero fiber curvature (a straight fiber) producing the lowest pullout forces. Fiber curvature effects are more pronounced, however, for the Coulomb friction model than for the constant friction model because it considers radial compressive stresses at the fiber/matrix interface [27]. Model predictions of wavy CNT-contained composites indicate that increases in nanotube curvature raise the peak bridging stress but also decrease the average pullout lengths of wavy CNTs. The overall effect can be a reduction in toughness as nanotube curvature increases, depending on the chosen parameters, including interfacial friction properties, nanotube and matrix modulus, and even crack opening [28]. The continuum theory is often applied in the pullout test. Systemic analyses of the pullout behavior of a helical fiber from an elastic matrix via finite element method simulation have been presented previously, with the implications regarding the underlying toughening mechanism of helicoid microstructures. Through their uniform curvature and torsion, helical fibers can provide a high pullout force and large interface areas, resulting in high energy dissipation that accounts, to a large extent, for the high toughness of biological materials [29]. An analytical fiber pullout model tailored for carbon nanotube reinforced polymer composites has been developed based on some classical models. Results show that the required axial stress to pull out a straight CNT at cryogenic temperatures is more than six times greater than that required at room temperature. Some other parameters, such as the length of a CNT and the modulus of the polymer, also influence the stresses in the CNT/polymer model [30]. The shear-lag model of CNTs is performed in the context of linear elasticity for axisymmetric problems. The numerical results reveal that the nanotube aspect ratio is a critical controlling parameter for nanotube-reinforced composites [31]. However, many assumptions introduced in these analytical studies undermine the accuracy of their findings by neglecting the discrete nature of CNTs and assuming CNTs to be homogenous, linearly elastic, and isotropic. MD is an effective method to deal with the problem without these unnecessary assumptions [32–34]. It has been widely applied to investigate the interfacial properties between polymer and nanocarbon materials, such as single-layer graphene [35], double-layered graphene [36], functionalized graphene [37], flattened carbon nanotubes [38], functionalized carbon nanotubes [39], multi-walled carbon nanotubes [40], CNT bundles [41], multi-walled carbon nanotubes [42], and single-layer diamonds [43]. The results prove that MD can simulate the interfacial properties with high precision and analyze the underlying toughening mechanism. A series of pullout simulations of carbon nanotubes has been carried out to investigate the interfacial properties between a CNT and a polymer matrix for two-phase CNT/polymer nanocomposites with only consideration of van der Waals interaction. The effects of nanotube length, diameter, and wall number on the pullout processes are studied, which indicates that the pullout force related to interfacial

properties is independent of nanotube length but is proportional to nanotube diameter [33]. The work is further extended using united-atom molecular dynamics [34] and an atomistic-based continuum multiscale modeling technique [44]. Using MD, the interfacial properties have been investigated. The pullout force of the wavy CNTs is significantly higher than its straight counterpart and rises further with the increase in the waviness of the CNTs. This is attributed to the added pullout energy dissipated in straightening the CNTs during the pullout process [45]. The key parameters influencing the ISS are the CNT radius, followed by the temperature and pulling velocity, respectively [46]. However, no molecular dynamics simulation has been carried out to examine the influence of geometric parameters of CCNTs on the interfacial properties of the CCNT/polymer interface by pullout tests to the best of our knowledge. Polyethylene (PE) is one of the most widely used organic materials [47] and is often used in the CNT composite [48–51]. Here, PE is adopted to represent the polymeric matrix.

This research investigates the application of CCNTs in the polymer composite for reinforcement. In Section 2, the pullout behavior of CCNTs and straight CNTs is simulated. The influence of parameters of CCNTs on the interface. The MD model is developed in Section 3. Finally, the conclusions of the present study are summarized in Section 4.

## 2. Results and Discussion

In the beginning, the CNT(6, 6) with a diameter of 8.14 Å is built and pulled out from the PE matrix. Figure 1 presents the pullout force versus the displacement. The pullout force quickly rises to the maximum force, and then it decreases until it becomes zero when the CNT is pulled out from the PE matrix. The ISS is 132 MPa, which is close to the result ISS = 134 MPa in previous research [33]. Further comparison of the CCNT/PE interface will be conducted in the following research after more experimental results are obtained.
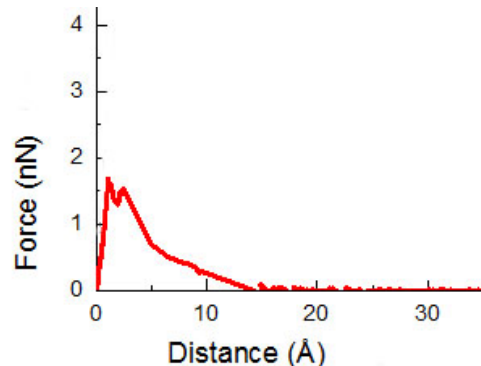


**Figure 1.** The pullout force versus displacement curve of the CNT with a diameter = 0.81 nm pulled out from the PE matrix.

Two MD simulations of the pullout test of the straight CNT and the CCNT were conducted to determine quantitatively the effect of shape on the pullout force and ISS. The pullout process is completed when the fully embedded nanotube is pulled out from the matrix. Figure 2 shows snapshots of the pullout simulation of a straight CNT. The CCNT, which has the same tube diameter as the straight CNT, is pulled out in Figure 3. The corresponding geometry and numerical results are displayed in Table 1.
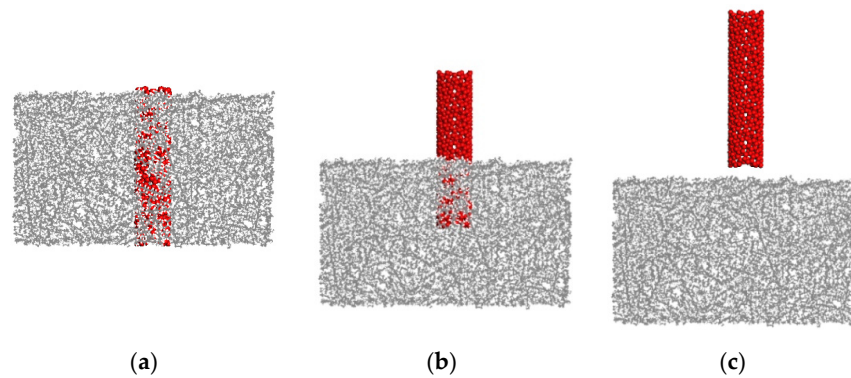
**Figure 2.** Snapshots of the CNT/PE composite during the pullout process. (**a**) 0 Å (**b**) 25 Å (**c**) 55 Å.
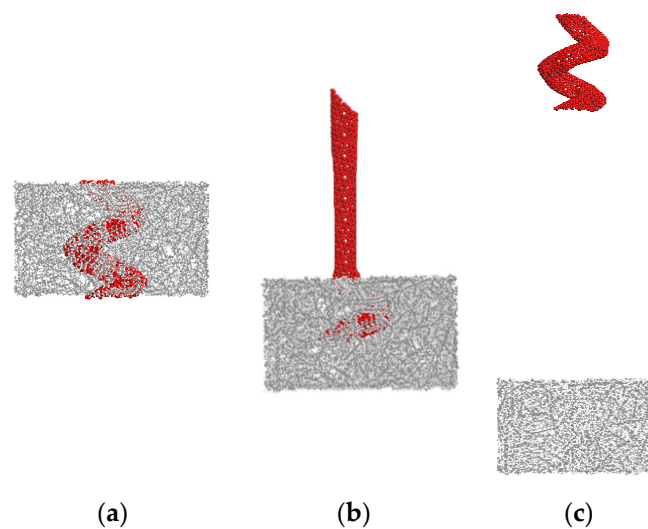


**Figure 3.** Snapshots of the CCNT/PE composite during the pullout process. (**a**) 0 Å (**b**) 80 Å (**c**) 200 Å.

**Table 1.** Geometries and pullout results for the straight CNT and the CCNT.

| Case # | Type | Outer Diameter ($D_t$) (Å) | Helix Angle ($\alpha$) (°) | Tube Diameter ($d_c$) (Å) | Inner Diameter ($D_c$) (Å) | Maximal Pullout Force (nN) | ISS (MPa) |
|--------|------|------|------|------|------|------|------|
| 2 | CNT | 11.3 | - | 11.3 | - | 1.946 | 127 |
| 3 | CCNT | 37.4 | 14.4 | 11.3 | 14.8 | 7.917 | 149 |

From Figures 2 and 3, the total length of the CCNT after being straightened is much longer than that of the straight CNT, even though the heights of RVE in the two cases are the same. The CCNT becomes straight during the pulling process, which consumes more energy considering that its initial configuration is coiled. The deformation of CCNTs contains three stages from Figure 3. Firstly, this pullout stage is characterized by the unfolding and stretching of the CCNT. Then, debonding occurs at the CCNT/matrix interface, beginning to propagate stably along the helical interface. When the crack length reaches a critical value, the crack propagation becomes unstable and usually leads to sudden interface debonding. Finally, frictional sliding of the CCNT begins until it is pulled out. The CCNT gradually restores its initial length and shape. After the CCNT is pulled out from the PE matrix in Figure 3c, it becomes coiled again.

Figure 4 shows the variation of the pullout force during the simulation. For straight CNTs, the applied pullout force is only responsible for overcoming the non-bonded interactions between the CNT's atoms and the surrounding polymer molecules. However, for CCNTs, additional work is required to overcome the resistance of the CCNT against shape

change and the accompanying change in the potential energy of the deformed CCNT. It can be seen from Figure 4 that a typical force–displacement curve of the pullout process of the CCNT includes three regions, which are similar to those found in Figure 3. During the unfolding and stretching of the CCNT, the elastic section is witnessed and no damage occurs in the beginning. Then, cracks occur at the CCNT/PE interface and quickly propagate after the pullout force increases to a certain value, resulting in a generally fluctuating force–displacement relationship. The crack propagation leads to a sudden interfacial debonding, which causes a decrease in the tensile force. Finally, the tensile force gradually reduces and fluctuates around 0 nN since the frictional sliding of the CCNT continues until the CCNT is pulled out. Previous experimental results showed that CCNT/polymer composites were much stiffer than straight CNT/polymer composites [6]. The interfacial properties may be influenced by many factors. This phenomenon can be well explained by the current model. Since CCNTs are more difficult to pull out, the stress transfer efficiency between CCNT/polymer composites is better than that in straight CNT/polymer composites. CCNTs are able to significantly increase the interfacial shear strength because of strong mechanical interlocking effect. It consequently leads to a greater stiffness in CCNT/polymer composites. Hence, CCNTs are very effective reinforcement for polymers.
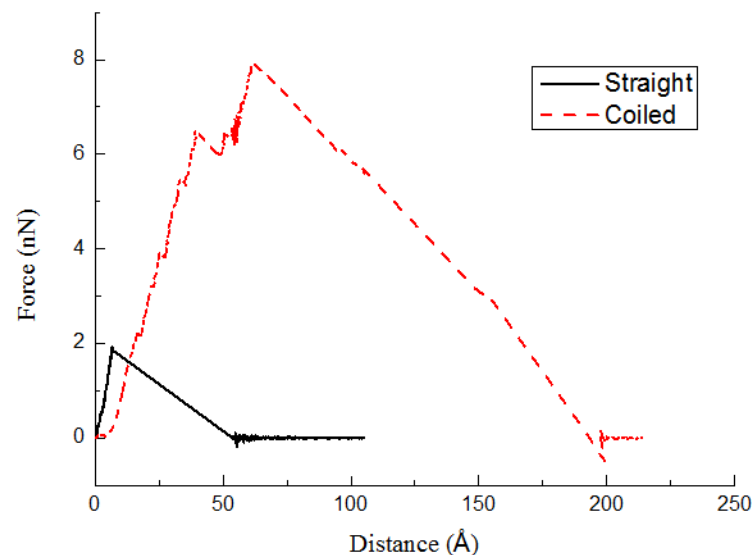


**Figure 4.** Variation of pullout force throughout the pullout process of CCNTs from the PE matrix.

The pullout force required to debond CCNTs can be simply described by adding a force $F_{coil}$ induced by CCNTs onto the force responsible for overcoming the van der Waals interactions as displayed in Equation (1).

$$F_{pull\text{-}out} = F_{vdW} + F_{coil} \tag{1}$$

There are many factors influencing the $F_{coil}$. Firstly, with the curvature, there is a component of force in the CCNT towards the center of the cycle as displayed in Figure 5a. Hence, the distance $d_1$ in Figure 5a is less than $d_2$ in Figure 5b. Decreasing the distance between the CCNT and the PE matrix tends to increase the interaction in that area. Hence, the interactions between the CCNT and PE are greater than those between the straight CNT and PE, which influences and contributes to $F_{coil}$. Secondly, an extra force is needed to straighten the CCNT during the pullout process, as shown in Figure 3b, which raises the tensile force. Thirdly, in contrast to a straight CNT, each section of the CCNT is subjected to twisting, bending, and axial extension deformations due to the curvature and torsion, leading to a complex stress field. The curvature and torsion of the CCNT induce a combination of the axial shear stress and the circumferential shear stress, which generates a much higher pullout force than that of the straight CNT.
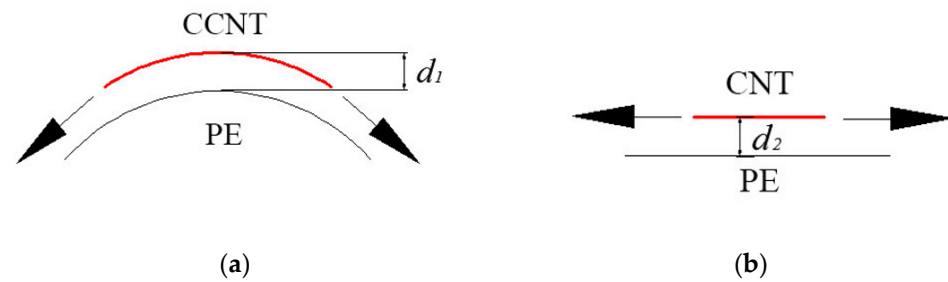
**Figure 5.** The CCNT and straight CNT on the PE matrix. (**a**) CCNT (**b**) CNT.

It is clear that the area below the force–displacement curve of the CCNT/PE composite is much greater than that of the CNT/PE composite from Figure 4. The helical shape leads to the greater length of the CCNT after it is straightened. Hence, the actual area between the CCNT and the matrix is much greater than that between the CNT and the matrix. Meanwhile, the tensile force in the CCNT/PE interface is greater than that in the CNT/PE interface from the above analysis. Considering these factors, the helical shape of the CCNT results in greater energy dissipation during the pullout process of the CCNT, even several times greater than that of the CNT reinforced composite. In CNT reinforced composites, the energy dissipation of CNTs during the pullout process is the main contributor to the toughness of the composite. Therefore, the helical shape of a CCNT at the microscale can be considered as one of the main sources of the high toughness of the CCNT reinforced composite.

The obtained pullout force from Equation (1) can be used to calculate the ISS. Table 1 summarizes the results obtained in two different cases. The ISS is also noted to rise in the CCNT/PE interface from Table 1. The ISS of the CNT/PE interface is 127 MPa, which is in good agreement with the value of 128 MPa calculated by Li et al. [33]. The additional interactions arosing from the added CCNTs significantly improve the peak pullout force and produce those observed characteristics in simulations.

### 2.1. Effect of Inner Diameters of the CCNT

The inner diameter of a CCNT affects its macroscopic reinforcement properties. Here, three cases are investigated. The geometry of related CCNTs and the summary of the pullout results are listed in Table 2. An initial comparison of the pullout profiles for all three inner diameters of CCNTs is displayed in Figure 6. The smaller inner diameters significantly improve the peak pullout force and produce the profiles in Figure 6. As the inner diameter increases, the ISS decreases from Table 2. The ISS in case 4 is 1.17 times as large as that in case 6. It demonstrates the advantage of using CCNTs with small inner diameters due to their significantly higher ISS values. The reason is that the inner diameter of CCNTs influences $F_{coil}$. When the inner diameter of CCNTs increases, the number of cycles of the CCNT decreases since $l_{tot}$ is determined. Since an extra force is needed to straighten the CCNT, less tensile force is required with fewer cycles. On the other hand, with larger inner diameters, the curvature decreases. Hence, the distance between the CCNT and the polymer matrix increases as displayed in Figure 5b. The interactions decrease, which results in a reduced tensile force. The trend is in good agreement with the corresponding results for wavy CNTs [27].

**Table 2.** Pullout force and ISS for different inner diameters.

| Case # | Outer Diameter $(D_t)$ (Å) | Helix Angle $(\alpha)$ (°) | Tube Diameter $(d_c)$ (Å) | Inner Diameter $(D_c)$ (Å) | Maximal Pullout Force (nN) | ISS (MPa) |
|---|---|---|---|---|---|---|
| 4 | 32.6 | 16 | 11.3 | 10 | 7.35 | 155 |
| 5 | 36.6 | 16 | 11.3 | 14 | 6.61 | 142.1 |
| 6 | 37.4 | 16 | 11.3 | 14.8 | 6.167 | 132.5 |

### 2.2. Effect of the Helix Angle

Figure 7 shows that the maximal pullout force distinctly decreases with the increasing helix angles. Related parameters of CCNTs are illustrated in Table 3. The helix angle denotes the degree of helicity of the CCNT. It also controls the total length of CCNTs ($l_{tot}$) embedded in the PE matrix with a fixed RVE height. Such results suggest that the greater helicity of the CCNT (i.e., smaller helix angles) can effectively enhance the maximal pullout force. Correspondingly, variations of the ISS are given in Table 3. The behavior of CCNTs is different from that in previous research with straight CNTs [16]. In previous research, the pullout profiles show very little variability, and the maximum pullout force is identical for different lengths. It can be inferred that the maximum pullout force remains relatively unchanged for CNTs with different lengths [16]. However, in the present research, the maximal tensile force of CCNTs increases with the reduced helix angle. The $F_{coil}$ is related to the total length of the CCNT embedded in the matrix. The CCNT/PE interface debonding force and the friction force increase with the CCNT length. With a greater $l_{tot}$, more atoms in CCNTs interact with the PE matrix, which causes a larger interface. Hence, a greater tensile force is required to pull the CCNT out of the PE matrix. The trend is in good agreement with the corresponding results for wavy CNTs [27]. During the pullout process, the debonding of the CCNT/PE interface and the subsequent frictional sliding between CCNTs and the PE matrix consume energy. The CCNT with smaller helix angles consumes a larger amount of energy according to Figure 7, which means greater toughness when the CCNT with a smaller helix angle is adopted. The results in Table 3 indicate that the helix angle of the CCNT can also effectively influence the values of ISS. With the increased helix angles, the number of cycles of the CCNT decreases. A smaller force is required to straighten the CCNT. Hence, the ISS decreases. It also demonstrates the advantage of using CCNTs with small helix angles due to their significantly higher ISS values.
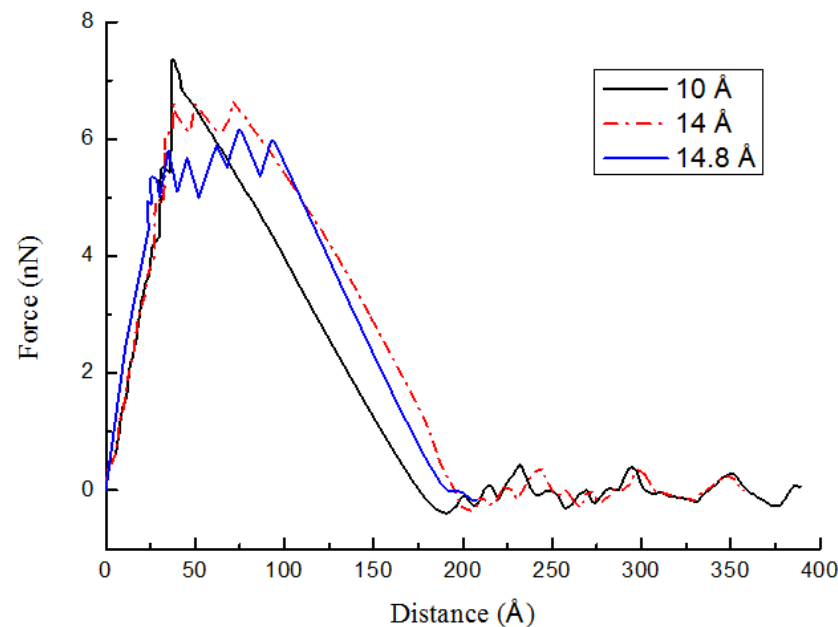


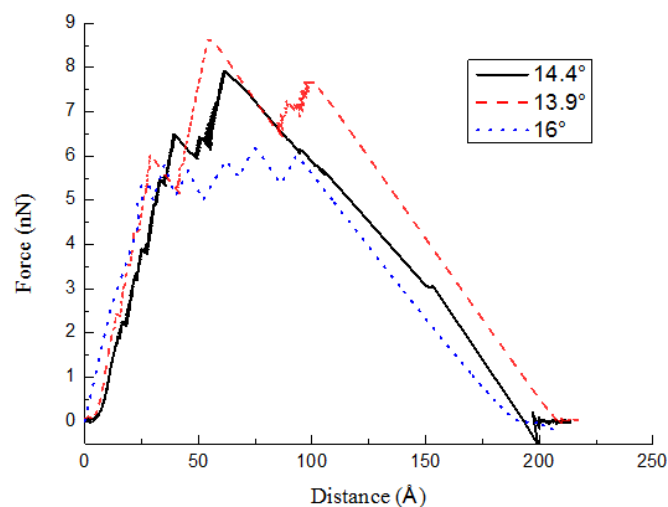**Figure 6.** Pullout profiles for CCNTs with different inner diameters.

**Figure 7.** Pullout force–displacement curves for different helix angles.

**Table 3.** Pullout force and ISS for different helix angles.

| Case # | Outer Diameter $(D_t)$ (Å) | Helix Angle ($\alpha$) (°) | Tube Diameter $(d_c)$ (Å) | Inner Diameter $(D_c)$ (Å) | Maximal Pullout Force (nN) | ISS (MPa) |
|---|---|---|---|---|---|---|
| 6 | 37.4 | 16 | 11.3 | 14.8 | 6.167 | 132.5 |
| 7 | 37.4 | 14.4 | 11.3 | 14.8 | 7.917 | 149 |
| 8 | 37.4 | 13.9 | 11.3 | 14.8 | 8.631 | 153.8 |

*2.3. Effect of the Tube Diameter*

The size of the nanotube cross-section also distinctly influences the pullout behaviors of the CCNT. In Figure 8, the force–displacement curves with different tube diameters are plotted. Here, cases 9, 10, and 11 are investigated. Related geometric parameters of CCNTs are listed in Table 4. It can be found that the maximal tensile force of the pullout process goes up by increasing the cross-section size. In previous research, a greater diameter of straight CNTs increases the pull-out force [33]. The trend is in good agreement with the corresponding results for straight CNTs [33]. Meanwhile, the slope of the force–displacement curves rises with the tube diameters in Figure 8. The area below the force–displacement curves when $d_c = 0.95$ nm is greater than that when $d_c = 0.82$ nm or 0.76 nm, which suggests that a larger nanotube causes greater toughness.
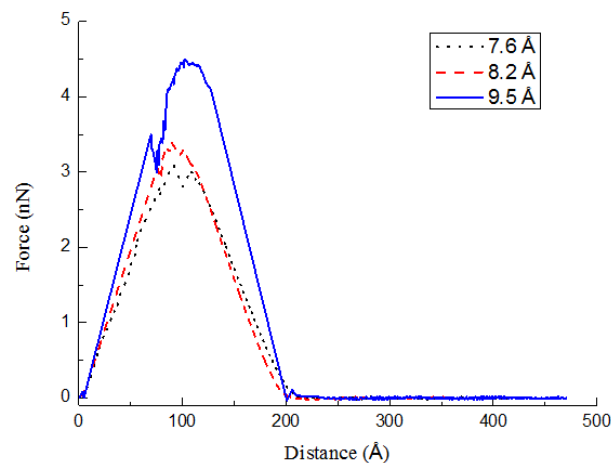


**Figure 8.** Pullout force–displacement curves for different diameters of CCNTs.

**Table 4.** Pullout force and ISS for different tube diameters.

| Case # | Outer Diameter ($D_t$) (Å) | Helix Angle ($\alpha$) (°) | Tube Diameter ($d_c$) (Å) | Inner Diameter ($D_c$) (Å) | Maximal Pullout Force (nN) | ISS (MPa) |
|--------|------|------|------|------|------|------|
| 9 | 29.4 | 14 | 7.6 | 14.2 | 3.12 | 168 |
| 10 | 30 | 14 | 8.2 | 13.6 | 3.32 | 163 |
| 11 | 29.5 | 14 | 9.5 | 10.5 | 4.45 | 160 |

The reason for the increase in the maximal tensile force mainly lies in that the tube diameter increases the interaction zone between the CCNT and PE, as shown in Figure 9. The PE molecules that are influenced by CCNT are exhibited as Zone 1 in Figure 9. The influenced PE molecules are more with larger tube diameters (see Figure 9a) than that with smaller tube diameters (see Figure 9b). On the other hand, it is easier to straighten a smaller tube than a larger tube. However, the ISS decreases with the rising tube diameter. The ISS is related to the interaction between one atom in the CCNT and the influenced PE matrix. The influenced PE molecules by one C atom are displayed as Zone 2 in Figure 9. Since the influenced atoms by one C atom in the CCNT are more in Figure 9d than in Figure 9c, the ISS goes up when the tube diameter reduces. This research may also contribute to other high-aspect ratio sustainable biomaterials, which are complementary alternatives to carbon nanotubes.
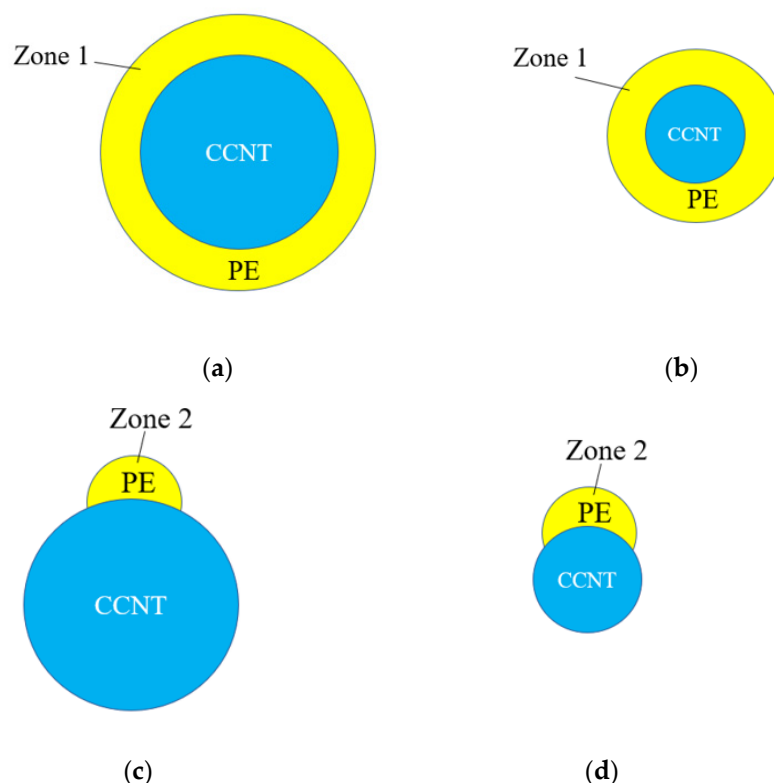


**Figure 9.** The CCNT and influenced PE matrix with different tube diameters. (**a**) Zone 1 of a large CCNT (**b**) Zone 1 of a small CCNT (**c**) Zone 2 of a large CCNT (**d**) Zone 2 of a small CCNT.

## 3. Methods and Materials

Here, the large-scale atomic/molecular massively parallel simulator (LAMMPS) is adopted in the MD simulations [52]. The adaptive intermolecular reactive empirical bond-order potential (AIREBO) is utilized in the interatomic interactions of carbon nanotubes [53]. The parameters of carbon atoms come from previous research [54–56]. The polymeric matrix is described by the united-atom model using the Dreiding force field, whose functional form and parameters are listed in Table 5 [57]. The Lennard–Jones potential is utilized in

the interatomic interaction between the PE and the CCNT. Table 5 shows the form and the parameters of the force field [54,58]. The cutoff is set at 10 Å [54].

**Table 5.** Function form of force field and potential parameters used for PE.

| Interaction | Form | Parameters |
|---|---|---|
| Bond | $E = \frac{1}{2}k_b(l - l_{eq})^2$ | $k_b = 2000$ kJ/mol Å, $l_{eq} = 1.53$ Å |
| Angle | $E = \frac{1}{2}k_\theta(cos(\theta) - cos(\theta_{eq}))^2$ | $k_\theta = 510$ kJ/mol, $\theta_{eq} = 110°$ |
| Torsional | $E = \frac{1}{2}\sum_{n=0}^{3} k_n cos^n \varphi$ | $k_0 = 14.477, k_1 = 37.594,$ $k_2 = 6.493, k_3 = 58.499$ (kJ/mol) |
| Non-bonded | $u = 4\varepsilon\left\{\left(\frac{\sigma}{r}\right)^{12} - \left(\frac{\sigma}{r}\right)^6\right\}$ | $\varepsilon = 0.468$ kJ/mol, $\sigma = 4.01$ Å, $r_c = 10.0$ Å |

*3.1. Modeling the CCNT/PE Interface*

In the beginning, atomistic models of CCNTs are constructed. One pair of pentagons and another pair of heptagons are first individually introduced in two sides of CNTs by adjusting the local topological structures of the two pairs of originally hexagonal rings as exhibited in Figure 10a. Pentagons form a cone defect, while heptagons result in a saddle defect, as is displayed in Figure 10b. Due to the strain energy induced by the pentagons and heptagons, the CNT becomes bent around the defect site after relaxation. A CCNT is formed based on the combination of basic structural segments. As illustrated in Figure 10c, two segments are connected to make the combined structure spiral. The structure in Figure 10c can be further used as a building block to construct complete CCNTs. By changing the tube length at the two ends of the basic segment or varying the nanotube diameter, different geometries of a CCNT are obtained. The CCNT exhibits a polygonal shape, which agrees with the experimental observation [59]. The periodic arrangement of pentagons and heptagons in the hexagonal network matches the features of the CCNT from previous research [60–62].



(**a**)       (**b**)       (**c**)
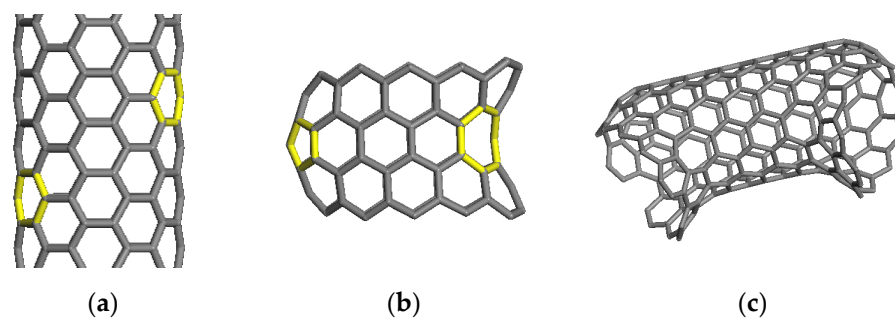
**Figure 10.** Procedures of constructing the CCNT model. The yellow rings are the introduced pentagons and heptagons. (**a**) Selecting the hexagonal rings (**b**) Introducing pentagons and heptagons (**c**) Final network.

By using the method mentioned above, the CCNT model can be constructed as displayed in Figure 11. The related parameters are also presented in Figure 11. The parameters are chosen based on previous literature [7]. Here, the inner diameter ($D_c$), the helix angle ($\alpha$) and the tube diameter ($d_c$) of CCNTs are investigated. The inner diameter ($D_c$) means the diameter of the inner cylinder, which is surrounded by the carbon nanocoil, and can be obtained by $D_c = D_t - 2dc$. $D_t$ means the outer diameter of the CCNT.
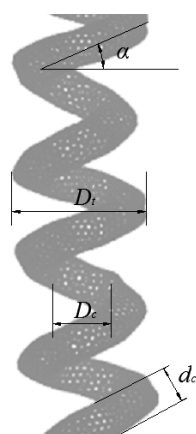
**Figure 11.** Geometrical parameters of a CCNT.

Then, a series of CNTs (i.e., cases 1 and 2) and CCNTs (i.e., cases 3–11) are built, which are illustrated in Table 6. Case 1 is modeled for comparison with previous research [33], which has a diameter of 8.14 Å. Two MD simulations of the pullout test of the straight CNT (i.e., case 2) and the CCNT (i.e., case 3) are conducted to determine quantitatively the effect of shape on the pullout force and ISS. Cases 4–6 are modeled to study the effect of the inner diameters of the CCNT. Cases 4–6 are modeled to investigate the effect of the helix angle. Cases 9–11 are modeled to explore the effect of the tube diameter. For the CCNT, the total length can be expressed as $l_{tot} = H_{RVE}/\sin(\alpha)$, where $H_{RVE}$ denotes the height of a representative volume element (RVE). After developing the CCNT model, the CCNT/PE interface model is built. Each RVE has one CCNT and 290 PE chains. Each PE chain contains 150 carbon atoms. The CCNT is set in the middle of the RVE as exhibited in Figure 12. The size of the RVE in each case is adjusted by forming the height as 5 nm. The total length of the CCNT after being straightened is about 20 nm, which is used in the pullout test with straight CNTs [44]. The width and length of the RVE are selected to be large enough so that the obtained results are independent of the size of the RVE. In the MD simulations, the periodic boundary condition is applied in *x-y* plane and the free boundary condition is assigned to *z* direction. In the z direction, a very large blank space is set to make room for the pulled-out CCNT.

**Table 6.** Parameters of CNTs and CCNTs.

| Case # | Type | Outer Diameter ($D_t$) (Å) | Helix Angle ($\alpha$) (°) | Tube Diameter ($d_c$) (Å) | Inner Diameter ($D_c$) (Å) |
|---|---|---|---|---|---|
| 1 | CNT | 8.14 | - | 8.14 | - |
| 2 | CNT | 11.3 | - | 11.3 | - |
| 3 | CCNT | 37.4 | 14.4 | 11.3 | 14.8 |
| 4 | CCNT | 32.6 | 16 | 11.3 | 10 |
| 5 | CCNT | 36.6 | 16 | 11.3 | 14 |
| 6 | CCNT | 37.4 | 16 | 11.3 | 14.8 |
| 7 | CCNT | 37.4 | 14.4 | 11.3 | 14.8 |
| 8 | CCNT | 37.4 | 13.9 | 11.3 | 14.8 |
| 9 | CCNT | 29.4 | 14 | 7.6 | 14.2 |
| 10 | CCNT | 30 | 14 | 8.2 | 13.6 |
| 11 | CCNT | 29.5 | 14 | 9.5 | 10.5 |
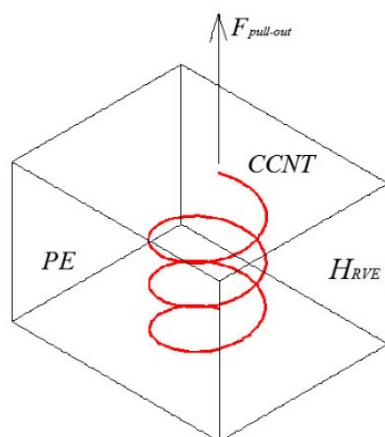
**Figure 12.** The RVE and the CCNT. The CCNT is shown in red.

### 3.2. MD Simulation Procedures

MD simulations of the pullout tests of CCNTs from the PE matrix are conducted by steered molecular dynamics [63]. A moving spring force is applied to the atoms at the head end of CCNTs [64] with the elastic spring constant $K_{\text{spring}}$ = 100 eV/Å$^2$ [46]. The tensile force of the pullout test can be recorded, as well as the displacement. The complete procedure for conducting the pullout simulations is illustrated as follows.

After modeling the CCNT and the polymetric matrix individually, the initial MD models of the PE and CCNTs are equilibrated by the conjugate gradient method [65]. The conjugate gradient method is one of the most popular and well-known iterative techniques for solving systems of sparsely symmetric positive definite linear equations. It is an important optimization algorithm and is widely adopted for structural optimization in MD. The energy-based stopping tolerance is set as etol = $10^{-30}$ and the force-based stopping tolerance is set as ftol = $10^{-30}$ eV/°A. More details can be found in previous research [66]. Then, the PE model and the CCNT model are put together. A specific number of the PE structures are dispersed randomly around a CCNT to build the nanocomposite using the Packmol package. Another PE model without the CCNT is also prepared as the control sample. The PE model without CCNTs is built just for the validation of the method with experimental results. After equilibrium, the density of the PE control sample without the CCNT is 0.83 g/cm$^3$, which is close to the data reported previously (c.f. Figure 3 in [67]). The calculated glass transition temperature (Tg) value is 252 K, which is in the experimental temperature range of 190–300 K in other research work [68,69]. The simulation domain is gradually compressed to the targeted size. At the beginning of each compression stage, the coordinates of all atoms are remapped to fit inside the updated domain. Then, the configuration is relaxed to reach equilibrium with the minimum potential energy. Geometry optimization of materials at the micro level is a prerequisite in most studies using molecular dynamics. The potential energy is a function of the coordinates of atoms. By changing the coordinate, the potential energy of the material can be minimized. This leads us to define the minimization problem. In the case of periodic systems, the geometry optimization is typically done using Cartesian coordinates. The number of degrees of freedom required for optimization is just $3N - 3$, where $N$ is the number of atoms in a single unit cell. The calculation is complete when the iterations have converged. They will be sufficiently close to their minimum structures, so that further full optimization only takes very few steps and the energetics will not change substantially. The complete description can be found in previous research [70]. The obtained system is further equilibrated at 300 K using the constant temperature and volume canonical (NVT) ensemble over 200 ps with 1 fs time step. Next, the equilibration is continued for another 200 ps by the isothermal-isobaric (NPT) ensemble at 300 K and 1 atm. The obtained system with the CCNT has a density of 1.0–1.1 g/cm$^3$, which is in accordance with previous research [71]. In this study, an agreement between the calculated physical properties of the MD models, i.e., density

and Tg value, and the experimental results indicates that the stable and equilibrated MD models are achieved. Three models with different initial configurations are built to obtain the average ISS of each case.

Finally, atoms at the head end of the CCNT are pulled out from the PE matrix at a constant velocity of $1 \times 10^{-4}$ Å/fs while the nanotube is equilibrated in the NVT ensemble at 300 K [72]. The configuration of the tensile simulation is displayed in Figure 12. The atoms of the polymer matrix are fixed during the pullout simulation [33]. The ISS is adopted as the representative of the interfacial properties between CCNTs and the polymer, which is calculated by [45,73]:

$$\text{ISS} = \frac{F_{pull-out}}{A_{interface}} = \frac{F_{pull-out}}{\pi d l_{tot}} \tag{2}$$

where, $F_{pull-out}$ is the maximum pullout force, $A_{interface}$ is the area of interfaces, $d$ is the diameter of tubes and $l_{tot}$ is the embedded CCNT length.

## 4. Conclusions

The pullout test of CCNTs has been simulated using MD to investigate the properties of the CCNT/PE interface. Different geometries of CCNTs, like the inner diameters, helix angles, and tube diameters, are considered. The results reveal that the maximal tensile force in the pullout tests is reduced by increasing CCNT inner diameters, increasing the helix angles and decreasing nanotube diameters. The distance between CCNTs and the polymer matrix is varied, and the less interfacial distance favors the greater ISS. Decreasing the inner diameter of the CCNT, the helix angle, and the tube diameter increases the ISS. The related enhancement mechanism has been illustrated. The present study helps to understand the interfacial adhesion behavior between polymers and CCNTs and is expected to contribute to the development of CCNT reinforced polymer composites. This research may also contribute to other high-aspect ratio sustainable biomaterials, which are complementary alternatives to carbon nanotubes. For example, fiber-reinforced composites (FRCs) [74] or cellulose nanocrystals (CNCs) [75] meet the criteria and can have potential applications in the preparation of composites for dentistry [76] and food packaging [77] fields, respectively.

In order to better understand the intermolecular interactions between neighboring CCNTs that eventually could influence the interfacial adhesion properties, the interaction between CCNTs should be considered in the pulling-out event. The dynamic simulation studies considering several CCNTs in the same pulling out event will be investigated in our following research.

**Institutional Review Board Statement:** Not applicable.

**Informed Consent Statement:** Not applicable.

**Data Availability Statement:** Data is contained within the article.

**Conflicts of Interest:** The authors declare no conflict of interest.

## References

1. Coleman, J.N.; Khan, U.; Blau, W.J.; Gun'ko, Y.K. Small but strong: A review of the mechanical properties of carbon nanotube–polymer composites. *Carbon* **2006**, *44*, 1624–1652. [CrossRef]
2. Liu, L.; Liu, F.; Zhao, J. Curved carbon nanotubes: From unique geometries to novel properties and peculiar applications. *Nano Res.* **2014**, *7*, 626–657. [CrossRef]

3.  Ansari, R.; Rouhi, S.; Eghbalian, M. On the elastic properties of curved carbon nanotubes/polymer nanocomposites: A modified rule of mixture. *J. Reinf. Plast. Comp.* **2017**, *36*, 991–1008. [CrossRef]

4.  Xie, J.; Mukhopadyay, K.; Yadev, J.; Varadan, V.K. Catalytic chemical vapor deposition synthesis and electron microscopy observation of coiled carbon nanotubes. *Smart. Mater. Struct.* **2003**, *12*, 744–748. [CrossRef]

5.  Chen, X.; Zhang, S.; Dikin, D.A.; Ding, W.; Ruoff, R.S.; Pan, L.; Nakayama, Y. Mechanics of a carbon nanocoil. *Nano Lett.* **2003**, *3*, 1299–1304. [CrossRef]

6.  Ma, H.L.; Jia, Z.; Lau, K.T.; Li, X.; Hui, D.; Shi, S.Q. Enhancement on mechanical strength of adhesively-bonded composite lap joints at cryogenic environment using coiled carbon nanotubes. *Comp. Part B Eng.* **2017**, *110*, 396–401. [CrossRef]

7.  Liu, X.; Yang, Q.S.; Liew, K.M.; He, X.Q. Superstretchability and stability of helical structures of carbon nanotube/polymer composite fibers: Coarse-grained molecular dynamics modeling and simulation. *Carbon* **2017**, *115*, 220–228. [CrossRef]

8.  Fakhrabadi, M.M.S.; Amini, A.; Reshadi, F.; Khani, N.; Rastgoo, A. Investigation of buckling and vibration properties of hetero-junctioned and coiled carbon nanotubes. *Comp. Mater. Sci.* **2013**, *73*, 93–112. [CrossRef]

9.  Ju, S.P.; Lin, J.S.; Chen, H.L.; Hsieh, J.Y.; Chen, H.T.; Weng, M.H.; Zhao, J.J.; Liu, L.Z.; Chen, M.C. A molecular dynamics study of the mechanical properties of a double-walled carbon nanocoil. *Comp. Mater. Sci.* **2014**, *82*, 92–99. [CrossRef]

10. Feng, C.; Liew, K.M.; He, P.; Wu, A. Predicting mechanical properties of carbon nanosprings based on molecular mechanics simulation. *Compos. Struct.* **2014**, *114*, 41–50. [CrossRef]

11. Ghaderi, S.H.; Hajiesmaili, E. Molecular structural mechanics applied to coiled carbon nanotubes. *Comp. Mater. Sci.* **2012**, *55*, 344–349. [CrossRef]

12. Ghaderi, S.H.; Hajiesmaili, E. Nonlinear analysis of coiled carbon nanotubes using the molecular dynamics finite element method. *Mater. Sci. Eng. A* **2013**, *582*, 225–234. [CrossRef]

13. Wu, J.; Nagao, S.; He, J.; Zhang, Z. Nanohinge-induced plasticity of helical carbon nanotubes. *Small* **2013**, *9*, 3561–3566. [CrossRef] [PubMed]

14. Tian, L.; Guo, X. Fracture and defect evolution in carbon nanocoil-A molecular dynamics study. *Comp. Mater. Sci.* **2015**, *103*, 126–133. [CrossRef]

15. Zaeri, M.M.; Ziaei-Rad, S. Elastic behavior of carbon nanocoils: A molecular dynamics study. *AIP Adv.* **2015**, *5*, 117114. [CrossRef]

16. Wernik, J.M.; Cornwell-Mott, B.J.; Meguid, S.A. Determination of the interfacial properties of carbon nanotube reinforced polymer composites using atomistic-based continuum model. *Int. J. Solids Struct.* **2012**, *49*, 1852–1863. [CrossRef]

17. Jiang, C.; Saha, A.; Martí, A.A. Carbon nanotubides: An alternative for dispersion, functionalization and composites fabrication. *Nanoscale* **2015**, *7*, 15037–15045. [CrossRef]

18. Gkikas, G.; Paipetis, A.S. Optimisation and analysis of the reinforcement effect of carbon nanotubes in a typical matrix system. *Meccanica* **2015**, *50*, 461–478. [CrossRef]

19. Cooper, C.A.; Cohen, S.R.; Barber, A.H.; Wagner, H.D. Detachment of nanotubes from a polymer matrix. *Appl. Phys. Lett.* **2002**, *81*, 3873–3875. [CrossRef]

20. Wagner, H.D.; Lourie, O.; Feldman, Y.; Tenne, R. Stress-induced fragmentation of multiwall carbon nanotubes in a polymer matrix. *Appl. Phys. Lett.* **1998**, *72*, 188–190. [CrossRef]

21. Wang, Z.J.; Kwon, D.J.; Choi, J.Y.; Shin, P.S.; Yi, J.W.; Byun, J.H.; Lee, H.I.; Park, J.K.; DeVries, K.L.; Park, J.M. Inherent and interfacial evaluations of carbon nanotubes/epoxy composites and single carbon fiber at different temperatures. *Comp. Part B Eng.* **2016**, *91*, 111–118. [CrossRef]

22. Zu, M.; Li, Q.; Zhu, Y.; Dey, M.; Wang, G.; Lu, W.; Deitzel, J.M.; Gillespie, J.W.; Byun, J.H.; Chou, T.W. The effective interfacial shear strength of carbon nanotube fibers in an epoxy matrix characterized by a microdroplet test. *Carbon* **2012**, *50*, 1271–1279. [CrossRef]

23. Tsuda, T.; Ogasawara, T.; Deng, F.; Takeda, N. Direct measurements of interfacial shear strength of multi-walled carbon nanotube/PEEK composite using a nano-pullout method. *Comp. Sci. Technol.* **2011**, *71*, 1295–1300. [CrossRef]

24. Chen, X.; Zheng, M.; Park, C.; Ke, C. Direct measurements of the mechanical strength of carbon nanotube–poly (methyl methacrylate) interfaces. *Small* **2013**, *9*, 3345–3351. [CrossRef] [PubMed]

25. Yazdchi, K.; Salehi, M. The effects of CNT waviness on interfacial stress transfer characteristics of CNT/polymer composites. *Compos. Part A Appl. Sci. Manuf.* **2011**, *42*, 1301–1309. [CrossRef]

26. Chen, X.; Beyerlein, I.J.; Brinson, L.C. Curved-fiber pull-out model for nanocomposites. Part 1: Bonded stage formulation. *Mech. Mater.* **2009**, *41*, 279–292. [CrossRef]

27. Chen, X.; Beyerlein, I.J.; Brinson, L.C. Curved-fiber pull-out model for nanocomposites. Part 2: Interfacial debonding and sliding. *Mech. Mater.* **2009**, *41*, 293–307. [CrossRef]

28. Chen, X.; Beyerlein, I.J.; Brinson, L.C. Bridged crack models for the toughness of composites reinforced with curved nanotubes. *J. Mech. Phys. Solids* **2011**, *59*, 1938–1952. [CrossRef]

29. Wang, L.; Cui, Y.; Qin, Q.; Wang, H.; Wang, J. Helical fiber pull-out in biological materials. *Acta. Mech. Solida. Sin.* **2016**, *29*, 245–256. [CrossRef]

30. Ma, H.L.; Lau, K.T.; Hui, D.; Shi, S.Q.; Poon, C.K. Theoretical analysis on the pullout behavior of carbon nanotube at cryogenic environment with the consideration of thermal residual stress. *Comp. Part B Eng.* **2017**, *128*, 67–75. [CrossRef]

31. Gao, X.L.; Li, K. A shear-lag model for carbon nanotube-reinforced polymer composites. *Int. J. Solids Struct.* **2005**, *42*, 1649–1667. [CrossRef]

32. Nam, K.H. Molecular dynamics-from macromolecule to small molecules. *Int. J. Mol. Sci.* **2022**, *23*, 5676. [CrossRef] [PubMed]

33. Li, Y.; Liu, Y.; Peng, X.; Yan, C.; Liu, S.; Hu, N. Pull-out simulations on interfacial properties of carbon nanotube-reinforced polymer nanocomposites. *Comp. Mater. Sci.* **2011**, *50*, 1854–1860. [CrossRef]

34. Wu, W.Q.; He, C.S.; Qiang, Y.B.; Peng, H.J.; Zhou, M.Y. Polymer-metal interfacial friction characteristics under ultrasonic plasticizing conditions: A united-atom molecular dynamics study. *Int. J. Mol. Sci.* **2022**, *23*, 2829. [CrossRef]

35. Shin, D.; Jeon, I.; Yang, S. Multiscale modeling assessment of the interfacial properties and critical aspect ratio of structurally defected graphene in polymer nanocomposites for defect engineering. *Eur. J. Mech. A-Solid* **2022**, *96*, 104728. [CrossRef]

36. Sahraei, A.; Mokarizadeh, A.; Foroutan, M.; George, D.; Rodrigue, D.; Baniassadi, M. Atomistic simulation of interfacial properties and damage mechanism in graphene nanoplatelet/epoxy composites. *Comp. Mater. Sci.* **2020**, *184*, 109888. [CrossRef]

37. Cui, J.; Zhao, J.; Wang, S.; Li, Y. A comparative study on enhancement of mechanical and tribological properties of nitrile rubber composites reinforced by different functionalized graphene sheets: Molecular dynamics simulations. *Polym. Compos.* **2021**, *42*, 205–219. [CrossRef]

38. Gaikwad, P.; Kowalik, M.; Jensen, B.; van Duin, A.; Odegard, G. Molecular dynamics modeling of interfacial interactions between flattened carbon nanotubes and amorphous carbon: Implications for ultra-lightweight composites. *ACS Appl. Nano Mater.* **2022**, *5*, 5915–5924. [CrossRef]

39. Song, Z.; Li, Y.; Yang, B. The interfacial load-transfer enhancement mechanism of amino-functionalised carbon nanotube reinforced epoxy matrix composites: A molecular dynamics study. *Compos. Sci. Technol.* **2021**, *209*, 108790. [CrossRef]

40. Cui, W.; Huang, W.; Hassan, H.; Cai, X.; Wu, K. Study on the interfacial contact behavior of carbon nanotubes and asphalt binders and adhesion energy of modified asphalt on aggregate surface by using molecular dynamics simulation. *Constr. Build. Mater.* **2022**, *316*, 125849. [CrossRef]

41. Kayang, K.; Banna, A.; Volkov, A. Chirality-dependent mechanical properties of bundles and thin films composed of covalently cross-linked carbon nanotubes. *Langmuir* **2022**, *38*, 1977–1994. [CrossRef] [PubMed]

42. Lyu, H.; Jiang, N.; Li, Y.; Lee, H.; Zhang, D. Enhanced interfacial and mechanical properties of carbon fiber/PEEK composites by hydroxylated PEEK and carbon nanotubes. *Compos. Part A Appl. S.* **2021**, *145*, 106364. [CrossRef]

43. Li, C.; Zhang, Z.; Zhan, H.; Zheng, Z.; Bai, J.; Gu, Y. Mechanical properties of single-layer diamond reinforced poly(vinyl alcohol) nanocomposites through atomistic simulation. *Macromol. Mater. Eng.* **2021**, *306*, 2100292. [CrossRef]

44. Alian, A.R.; Kundalwal, S.I.; Meguid, S.A. Interfacial and mechanical properties of epoxy nanocomposites using different multiscale modeling schemes. *Compos. Struct.* **2015**, *131*, 545–555. [CrossRef]

45. Alian, A.R.; Meguid, S.A. Molecular dynamics simulations of the effect of waviness and agglomeration of CNTs on interface strength of thermoset nanocomposites. *Phys. Chem. Chem. Phys.* **2017**, *19*, 4426–4434. [CrossRef]

46. Vu-Bac, N.; Lahmer, T.; Zhang, Y.; Zhuang, X.; Rabczuk, T. Stochastic predictions of interfacial characteristic of polymeric nanocomposites (PNCs). *Comp. Part B Eng.* **2014**, *59*, 80–95. [CrossRef]

47. Sertchook, H.; Elimelech, H.; Makarov, C.; Khalfin, R.; Cohen, Y.; Shuster, M.; Babonneau, F.; Avnir, D. Composite particles of polyethylene@ silica. *J. Am. Chem. Soc.* **2017**, *129*, 98–108. [CrossRef]

48. Kanagaraj, S.; Varanda, F.R.; Zhil'tsova, T.V.; Oliveira, M.S.; Simões, J.A. Mechanical properties of high density polyethylene/carbon nanotube composites. *Compos. Sci. Technol.* **2007**, *67*, 3071–3077. [CrossRef]

49. McNally, T.; Pötschke, P.; Halley, P.; Murphy, M.; Martin, D.; Bell, S.E.; Brennan, G.P.; Bein, D.; Lemoine, P.; Quinn, J.P. Polyethylene multiwalled carbon nanotube composites. *Polymer* **2015**, *46*, 8222–8232. [CrossRef]

50. Gou, J.; Liang, Z.; Zhang, C.; Wang, B. Computational analysis of effect of single-walled carbon nanotube rope on molecular interaction and load transfer of nanocomposites. *Compos. Part B Eng.* **2005**, *36*, 524–533. [CrossRef]

51. Yang, H.; Chen, Y.; Liu, Y.; Cai, W.S.; Li, Z.S. Molecular dynamics simulation of polyethylene on single wall carbon nanotube. *J. Chem. Phys.* **2007**, *127*, 094902. [CrossRef] [PubMed]

52. Plimpton, S. Fast parallel algorithms for short-range molecular dynamics. *J. Comp. Phys.* **1995**, *117*, 1–19. [CrossRef]

53. Brenner, D.W.; Shenderova1, O.A.; Harrison, J.A.; Stuart, S.J.; Ni, B.; Sinnott, S.B. A second-generation reactive empirical bond order (REBO) potential energy expression for hydrocarbons. *J. Phys.-Condens. Mat.* **2002**, *14*, 783–802. [CrossRef]

54. Zhang, Y.; Zhao, J.; Wei, N.; Jiang, J.; Gong, Y.; Rabczuk, T. Effects of the dispersion of polymer wrapped two neighbouring single walled carbon nanotubes (SWNTs) on nanoengineering load transfer. *Comp. Part B Eng.* **2013**, *45*, 1714–1721. [CrossRef]

55. Zhang, Y.; Zhuang, X.; Muthu, J.; Mabrouki, T.; Fontaine, M.; Gong, Y.; Rabczuk, T. Load transfer of graphene/carbon nanotube/polyethylene hybrid nanocomposite by molecular dynamics simulation. *Comp. Part B Eng.* **2014**, *63*, 27–33. [CrossRef]

56. Lu, Y.B.; Yang, Q.S.; He, X.Q.; Liew, K.M. Modeling the interfacial behavior of carbon nanotube fiber/polyethylene composites by molecular dynamics approach. *Comp. Mater. Sci.* **2016**, *114*, 189–198. [CrossRef]

57. Vu-Bac, N.; Lahmer, T.; Keitel, H.; Zhao, J.; Zhuang, X.; Rabczuk, T. Stochastic predictions of bulk properties of amorphous polyethylene based on molecular dynamics simulations. *Mech. Mater.* **2014**, *68*, 70–84. [CrossRef]

58. Capaldi, F.M.; Boyce, M.C.; Rutledge, G.C. Molecular response of a glassy polymer to active deformation. *Polymer* **2004**, *45*, 1391–1399. [CrossRef]

59. Zhang, X.F.; Zhang, Z. Polygonal spiral of coil-shaped carbon nanotubules. *Phys. Rev. B* **1995**, *52*, 5313–5317. [CrossRef]

60. Amelinckx, S.; Zhang, X.B.; Bernaerts, D.; Zhang, X.F.; Ivanov, V.; Nagy, J.B. A formation mechanism for catalytically grown helix-shaped graphite nanotubes. *Science* **1994**, *265*, 635–639. [CrossRef]

61. Bajpai, V.; Dai, L.; Ohashi, T. Large-scale synthesis of perpendicularly aligned helical carbon nanotubes. *J. Am. Chem. Soc.* **2014**, *126*, 5070–5071. [CrossRef] [PubMed]

62. Liu, L.Z.; Gao, H.L.; Zhao, J.J.; Lu, J.P. Superelasticity of carbon nanocoils from atomistic quantum simulations. *Nanoscale Res. Lett.* **2010**, *5*, 478–483. [CrossRef] [PubMed]

63. Isralewitz, B.; Gao, M.; Schulten, K. Steered molecular dynamics and mechanical functions of proteins. *Curr. Opin. Struc. Biol.* **2001**, *11*, 224–230. [CrossRef]

64. Büyüköztürk, O.; Buehler, M.J.; Lau, D.; Tuakta, C. Structural solution using molecular dynamics: Fundamentals and a case study of epoxy-silica interface. *Int. J. Solids Struct.* **2011**, *48*, 2131–2140. [CrossRef]

65. Saha, L.C.; Mian, S.A.; Jang, J.K. Molecular dynamics simulation study on the carbon nanotube interacting with a polymer. *B. Korean. Chem. Soc.* **2012**, *33*, 893–896. [CrossRef]

66. Darvishi, F.; Rahmani, O. Calibration of nonlocal generalized helical beam model for free vibration analysis of coiled carbon nanotubes via molecular dynamics simulations. *Mech. Adv. Mater. Struc.* **2022**, *1*, 247282721. [CrossRef]

67. Yi, P.; Locker, C.R.; Rutledge, G.C. Molecular dynamics simulation of homogeneous crystal nucleation in polyethylene. *Macromolecules* **2013**, *46*, 4723–4733. [CrossRef]

68. Awasthi, A.P.; Lagoudas, D.C.; Hammerand, D.C. Modeling of graphene–polymer interfacial mechanical behavior using molecular dynamics. *Mater. Sci. Eng.* **2018**, *17*, 015002. [CrossRef]

69. Han, J.; Gee, R.H.; Boyd, R.H. Glass transition temperatures of polymers from molecular dynamics simulations. *Macromolecules* **1994**, *27*, 7781–7784. [CrossRef]

70. Martínez, J.; Martínez, L. Packing optimization for automated generation of complex system's initial configurations for molecular dynamics and docking. *J. Comput. Chem.* **2003**, *24*, 819–825. [CrossRef]

71. Haghighatpanah, S.; Bohlén, M.; Bolton, K. Molecular level computational studies of polyethylene and polyacrylonitrile composites containing single walled carbon nanotubes: Effect of carboxylic acid functionalization on nanotube-polymer interfacial properties. *Front. Chem.* **2014**, *2*, 74. [CrossRef] [PubMed]

72. Yang, L.; Tong, L.; He, X. MD simulation of carbon nanotube pullout behavior and its use in determining mode I delamination toughness. *Comp. Mater. Sci.* **2012**, *55*, 356–364. [CrossRef]

73. Chawla, R.; Sharma, S. Molecular dynamics simulation of carbon nanotube pull-out from polyethylene matrix. *Compos. Sci. Technol.* **2017**, *144*, 169–177. [CrossRef]

74. Vallittu, P. High-aspect ratio fillers: Fiber-reinforced composites and their anisotropic properties. *Dent. Mater.* **2015**, *1*, 1–7. [CrossRef] [PubMed]

75. Marcuello, C.; Foulon, L.; Chabbert, B.; Molinari, M.; Aguie-Beghin, V. Langmuir-blodgett procedure to precisely control the coverage of functionalized AFM cantilevers for SMFS measurements: Application with cellulose nanocrystals. *Langmuir* **2018**, *34*, 9376–9386. [CrossRef]

76. Mena-Álvarez, J.; Agustin-Panadero, R.; Zubizarreta-Macho, A. Effect of fiber-reinforced composite and elastic post on the fracture resistance of premolars with root canal treatment-an in vitro pilot study. *Appl. Sci.* **2020**, *10*, 7616. [CrossRef]

77. Berzin, F.; Lemkhanter, L.; Marcuello, C.; Chabbert, B.; Aguie-Beghin, V.; Molinari, M.; Castellani, R.; Vergnes, B. Influence of the polarity of the matrix on the breakage mechanisms of lignocellulosic fibers during twin-screw extrusion. *Polym. Compos.* **2020**, *41*, 1106–1117. [CrossRef]